Ethyl acetate extracts of Bungeanum ameliorates cognitive deficits by suppressing NLRP3 inflammasome-dependent pyroptosis in aging mice

Meihuan Zhao
Chengdu University of Traditional Chinese Medicine Wenjiang Campus: Chengdu University of Traditional Chinese Medicine

Yuan Dai
Chengdu College of Traditional Chinese Medicine: Chengdu University of Traditional Chinese Medicine

Ping Li
Chengdu University of Traditional Chinese Medicine Wenjiang Campus: Chengdu University of Traditional Chinese Medicine

Jie Wang
Chengdu University of Traditional Chinese Medicine Wenjiang Campus: Chengdu University of Traditional Chinese Medicine

Tengyun Ma
Chengdu University of Traditional Chinese Medicine Wenjiang Campus: Chengdu University of Traditional Chinese Medicine

Shijun Xu (xushijun@cdutcm.edu.cn)
Chengdu University of TCM: Chengdu University of Traditional Chinese Medicine
https://orcid.org/0000-0002-7454-0873

Research

Keywords: Zanthoxylum bungeanum Maxim., cognitive deficit, ethyl acetate fraction, oxidative damage, pyroptosis, NLRP3 inflammasome

Posted Date: March 17th, 2021

DOI: https://doi.org/10.21203/rs.3.rs-303236/v1

Abstract

Background: The NLRP3-mediated pyroptosis is a key player in the development of the age-associated neurodegenerative disease. *Zanthoxylum bungeanum* Maxim (Rutaceae), a homologous of medicine and foodstuff, has previously been demonstrated the potential prevention of cognitive dysfunction in aging mice. However, it is still unknown which fraction is the material basis responsible for their therapeutic effects and whether *Z. bungeanum* could confer anti-cognitive deficits activity via restraining NLRP3-mediated pyroptosis. Thus, in the current study, we explored the active fraction of *Z. bungeanum* against cognitive deficits and its underlying mechanism.

Methods: In the present study, the D-galactose-induced mouse model of aging was established to explore the effect of cognitive impairment of four fractions of *Z. bungeanum*, including petroleum ether (PE), methylene chloride (DCM), ethyl acetate (EA), and n-butanol (N-BAI). We next activated the NLRP3 inflammasome in BV-2 microglia cells to investigate the mechanisms for the neuroprotective effect of the active fraction of *Z. bungeanum*.

Results: We demonstrated that the mice treated with EA had significantly alleviated the memory deficit induced by D-galactose. Meanwhile, EA up-regulated the cortex NeuN protein level, improved the survival and morphology of hippocampal neurons. We further found that EA significantly alleviated oxidative damage, inhibited activation of microglia, and suppressed NLRP3 inflammasome activation and subsequent cleaved Caspase-1, IL-1β, IL-18, and GSDMD-N. Correspondingly, in vitro data showed that EA protected BV-2 cells against Lipopolysaccharide (LPS) and adenosine triphosphate (ATP) elicited NLRP3 inflammasome activation and pyroptosis, evidenced by declined the protein levels of NLRP3, cleaved Caspase-1, IL-1β, IL-18, and GSDMD-N. These data indicated that EA inhibited NLRP3-mediated pyroptosis.

Conclusions: Our work revealed that the EA active fraction of *Z. bungeanum* protected neurons from inflammation through inhibition of NLRP3 and subsequent pyroptosis in microglia, and suggested promising clinical use of EA for age-associated neurodegenerative disease.

Background

Aging, the natural complex, and inevitable physiological phenomenon across the lifespan is the major factor underlying cognitive disorders and related to age-related neurodegenerative disorders, such as Alzheimer's disease (AD), Parkinson's disease (PD) [1]. According to the world population prospects of the United Nations, the proportion of older people (aged 60 or above) has been estimated that will reach 20% by 2050 and brought great attention worldwide [2]. Dysfunction of the antioxidant defense system, neuroinflammation, and DNA lesion was involved in the aging brain, increasing the incidence rate of neurodegenerative diseases [3]. Hence, preventing neuroinflammation-induced neuronal degeneration might be a potential neurotherapeutic approach in treating age-associated neurodegenerative disease. D-galactose (D-gal) can mimic aging in animal models by inducing oxidative stress and neuroinflammation,

experimentally, the ROS and neuroinflammatory cascades can be substantially replicated by lipopolysaccharide- (LPS-) stimulated BV-2 microglial cells (in vitro) [12]. Thus, these models have been adapted to investigate the therapeutic potential for various bioactive candidates in neurodegenerative diseases.

Microglia, the resident innate immune cells of the central nervous system, which-mediated neuroinflammation is one of the major pathological hallmarks of the occurrence of age-associated neurodegenerative diseases [4]. NLR3 family pyrin domain containing 3 (NLRP3) inflammasomes is crucial for the neuroinflammatory response as sensors of cell pressure and invading pathogens [5]. Reactive oxygen species (ROS), metabolic stress, and damage-associated molecular patterns can activate NLRP3 inflammasome, regulating the activation of caspase-1 and promoting the production of potent pro-inflammatory cytokines that augment inflammatory cell injury [6, 7]. Assembly of the inflammasome activates the cysteine protease caspase-1, leading to the proteolytic cleavage of the proinflammatory cytokines Interleukin-1β (IL-1β), Interleukin-18 (IL-18), and the pore-forming protein gasdermin D (GSDMD) causing pyroptosis, which a newly discovered programmed cell death initiated by inflammasomes that different from apoptosis and necrosis [8, 9]. These cascades eventually result in neuronal loss, as has been observed in the aging brain [10, 11].

Plants are the primary sources of food and drugs for humans, and previous studies have revealed that the extracts of medicinal and edible homologous plants, such as ginseng, are sold as supplements to improve cognitive function [13]. The importance of a reasonable diet for cognitive protection was pointed in the Lancet Commission 2020 [14]. *Z. bungeanum*, belonging to the Rutaceae family, is a kind of medicinal and edible plant widely distributed throughout East Asian countries, including China, Japan, and Korea [15]. It is widely used as a popular spice and one of the eight essential Chinese traditional sauces in cooking because of its unique spicy taste and flavor. In addition, *Z. bungeanum* is a commonly used herbal medicine in China with effects of anti-inflammatory, analgesic, antibacterial, and improving learning and memory ability [16]. In our previous work, it has proved that *Z. bungeanum* could relieve oxidative damage and cognitive dysfunction in aging mice [17]. However, the material basis and mechanisms by which *Z. bungeanum* are not fully understanding.

This study aims to elucidate the age-related cognitive decline effects of *Z. bungeanum* different polar fractions, identify the active fraction and the possible underlying mechanisms of it. The adequate and reliable data indicated beneficial to prevent and improve age-related cognitive decline, oxidative damage, and neuroinflammation via intake of EA fraction of *Z. bungeanum*, meanwhile provide a convincing foundation to develop ingredients of *Z. bungeanum*.

Material And Methods

2.1 Chemicals, reagents, and materials

Z. bungeanum Maxim. (Catalog No. 20180802) was purchased from Hehuachi tradition herbal medicine market (Chengdu, China). D-galactose (D-gal, Catalog No. 2018070901) was provided by Cologne

Chemical Co., Ltd (Chengdu, China). Lipopolysaccharides (LPS, Catalog No. 032M4082V) was purchased from Sigma-Aldrich (St. Louis, USA). Adenosine 5'-triphosphate disodium salt (ATP, Catalog No. S0714A) was purchased from Meilun Biotechnology Co., Ltd (Dalian, China). Hydergine (Catalog No. 6G862T) was provided by Huajin Pharmaceutical Co., Ltd (Tianjin, China). Baicalin (Catalog No. 20170319) was obtained from Biological Engineering Co., Ltd (Xi'an, China). The primary antibodies including anti-caspase-1, anti-GSDMD, and anti-NLRP3 (Catalog No. 36458S, 67314S, 15101S) were from Cell Signaling Technology (Beverly, USA); anti-IL-1β (Catalog No. 510681) was from Zhengneng Biotechnology Co. LTD (Chengdu, China); anti-IL-18 (Catalog No. GR3285548-4) was from Abcam (Cambridge, UK); anti-ionized calcium binding adapter molecule 1 (anti-Iba1), anti-Mac-1, alphaM integrin, Cr3, MO-1, C3bi Receptor (anti- CD11b) (Catalog No. #18m3752, #DF2911) were from Affinity Biosciences, Inc (Cincinnati, OH, USA). Superoxide dismutase kit (SOD, Catalog No. 20180605), malondialdehyde kit (MDA, Catalog No. 20180611) were obtained from Jiancheng Bioengineering Institute (Nanjing, China). Tunel kit (Catalog No. XZ201902) was from Seville Biotechnology Co., Ltd (Wuhan, China). Cell culture medium, double antibody and serum were purchased from Gibco (Grand Island, NY). All organic reagents were purchased from Kelong Chemical Co., Ltd (Chengdu, China).

2.2 Preparation of extraction

Solvents of four different polarities solvents (petroleum ether, dichloromethane, ethyl acetate and n-butanol) were used to fractionate *Z. bungeanum* extracts. The dried *Z. bungeanum* (500 g) was soaked in 5000 mL 95% ethanol for 24h and then filtered it. We repeated this operation one more time, and transferred the filtrate to a flask for evaporation. After the liquid was concentrated to 400 ml, we used petroleum ether, dichloromethane, ethyl acetate and n-butanol were used for extraction twice in turn. These filtrates were concentrated by rotary evaporator. Finally, each extract was collected in a screw tube and kept them in a vacuum desiccator for 3–5 days to completely remove each organic solvent. The extracts were away from light stored at 4 °C until use. We referred to the fraction with petroleum ether as PE, the fraction with dichloromethane, as DCM, the fraction with ethyl acetate, as EA, and the fraction with n-butanol, as N-BAI.

2.3 Animals

Male Kunming mice (8 weeks old) were purchased from the Dashuo Experimental Animal Co., Ltd and housed under suitable conditions of temperature (22 ± 2℃) and humidity (65 ± 5%) in the animal observation room of Chengdu University of Traditional Chinese Medicine with free access to water and food. All animal experiments were performed according to the National Institutes of Health Guide for the Care and Use of Laboratory Animals, and the Institute of Material Medica Integration and Transformation for Brain Disorders ethics committee approved the animal protocols. Mice were randomly divided into seven groups (n=6 in each group): solvent plus saline (control group), solvent plus D-gal (aging group), 0.9 mg/kg Hydergine plus D-gal (HG group), PE plus D-gal (PE group), DCM plus D-gal (DCM group), EA plus D-gal (EA group), and N-BAI plus D-gal (N-BAI group). Drugs were dissolved in 0.5% CMC-Na for administration, and the dose of each extract was equal to 450 mg/Kg of raw material. After oral

administration of the for 1 h, 500 mg/kg D-gal was subcutaneously injected once a day for 42 days. After that, all the animals were executed for further study.

2.4 Behavioral evaluation

The protocol followed the sequence of passive avoidance test and Morris water maze test. All tests were performed in conditions of dim light and low noise. The passive avoidance test was performed as previously described [18]. The test was performed daily for 2 consecutive days, and the first day was the training trial, and the second day was the test trial. Mice were individually placed into the apparatus and permitted free exploration for 5 min. The mice were individually placed in a lit room and allowed free access to the corresponding dark room when a trap door was opened. The latency time taken to pass through the trap door was recorded as " Escape latency ", and the number of times the mice passed through the trap door was counted as " The number of errors ". If the mouse did not pass through the trap door within 300 s, a latency of 300 s was recorded.

The Morris water maze test was conducted based on earlier methodology [18]. In the orientation navigation experiment, the mice were placed in the opposite quadrant of the platform and allowed to swim until it found the hidden platform within 60 s. The time of finding the platform was recorded as" Escape latency ". If the mice could not find the platform within 60 s, it was gently guided to the platform and kept there 10 s, and the was recorded as 60 s. The continuous period of the hidden platform experiment was 5 days. Next the spatial probe trial was performed by removing the platform on the sixth day. The swimming time in target quadrant and the number of crossing the platform were recorded in the spatial probe trial.

2.5 Hematoxylin and eosin staining

For hematoxylin and eosin (HE) staining, four mice brain samples in each group were collected and postfixed in 4% paraformaldehyde. The hemisphere of each mouse was embedded in paraffin and cut into 4 μm slices, dewaxed, which were then stained successively with hematoxylin and eosin to observe lesions in the hippocampus. And only large intact cells with clearly stained cytoplasm and a distinct nucleus, usually with evident nucleoli, were counted as healthy neurons [19].

2.6 Immunohistochemistry

Immunohistochemistry of the paraffin blocks were performed as previously described [20]. The brain slices were dewaxed, rehydrated, blocked, incubated with primary antibodies (NeuN,1:500, Iba-1,1:200) overnight for 4°C, incubated with secondary antibody and colored with a DAB kit.

2.7 Measurement of the activity of SOD and the content of MDA

The activity of SOD and the content of MDA were determined strictly according to the kit instructions.

2.8 Tunel staining

The paraffin blocks were cut into 4 μm slices, dewaxed, repaired with proteinase K working solution, disrupted cytomembrane, incubated with TdT and FITC-12-dUTP for 1 h. After rinsing with phosphate-buffered solution (PBS), the nuclei were stained with DAPI, then anti-fluorescence quenching agent was added. Then the samples were observed immediately under fluorescence microscope after sealed with neutral balsam on slides. Pay attention to avoid light in the experiment.

2.9 Cell culture and Cell viability measurements

BV-2 microglial cells were purchased from Chinese Academy of Sciences (shanghai, China). Cells were cultured in Dulbecco's modified Eagle's medium (DMEM) with 10% fetal bovine serum and 1% streptomycin/penicillin, maintained at 37°C under 5% CO2. Cells in the exponential growth phase were used for all experiments. Cells were plated into 96-well plates at a density of 1×10^4 or plated into 6-well plates at 1×10^5 densities. After culturing for 24h, drugs were first added for 1h, then 100 ng/ml LPS was added for 12 h, and finally, ATP (2.5 mM) was added for 3h. After the cells were treated as described above, 10μl of MTT solution was added to each well. Finally, after the plates were incubated in the incubator for 4h, remove the supernatant, add dimethyl sulfoxide, incubate in a shaker, and absorbance was measured at 490 nm. Cell experiments were independently performed at least three times.

2.10 Western blotting

Tissues and collected cells were lysed with lysate, centrifuged, collected supernatant, added with sample buffer, and stored at -80℃. SDS-PAGE was used to isolate proteins, then the protein was transferred to PVDF membrane，blocked with 5 % skimmed milk, incubated with primary antibodies (cleaved GasderminD,1:1000; Cleaved Caspase-1,1:1000; NLRP3, 1:500; IL-1β, 1:1000; IL-18, 1:1000; GAPDH, 1:5000) overnight at 4℃,and the second antibody were incubated the next day. Finally, the relative expression of the target protein was analyzed by the Quantity One software.

2.11 Sample preparation and Mass spectrometry analysis

EA fraction was extracted with methanol solution by ultrasonic extraction, and filtered through a 0.22 μm micropore film to yield the sample solution for HPLC-MS/MS. The sample was analyzed by an Agilent Technologies 1290 LC and an Agilent Technologies 6410 triple quadrupole mass spectrometer (Agilent Technologies, CA, USA). And the chromatographic separation was performed on a poroshell 120 EC-C18 column (100 × 4.6 mm, 2.7 μm, Agilent Technologies, CA, USA) at 29°C. The mobile phase consisted of H2O (containing 0.05% formic acid, A) and acetonitrile (B) in the gradient elution program: 0 ⟶ 3 min, 5% ⟶ 18% B; 3 ⟶ 10 min, 18% B; 10⟶ 20 min, 18% ⟶ 63% B. The flow rate was 0.3 mL/min, and the sample injection volume was 10 μL. Mass spectrometric scan was obtained by electrospray ionization (ESI) in positive-ion mode with a scanning interval m/z 100–1300. The main parameters for MS were set as follows: gas temperature, 300 °C; gas flow, 11L·min^{-1}; nebulizer, 35 psig; capillary voltage, 4000 V; and atomizer pressure 15 psi (1 psi = 6.895 Kpa).

2.12 Statistical analysis

All dates are represented as the mean ± standard error of the mean (SEM). The escape latency in the Morris water maze test navigation phase was analyzed by two-way analysis of variance (ANOVA). For other data, date with a normal distribution was analyzed by one-way ANOVA. Student's test was performed for comparisons between two groups. And Bonferroni *post hoc* analysis was conducted, and the statistical significance was tested at $P < 0.05$.

Results

3.1 Effects of four different polarities fractions of Z. bungeanum on cognitive impairment in aging mice.

The Passive avoidance test was first used to evaluate the effects of PE, DCM, EA, and N-BAI fractions on fear memory disorder in aging mice induced by D-gal (Fig. 1A and 1B). There was no significant difference among the groups during the training for the escape latency and the number of errors. However, in the testing trial, compared with control mice, the escape latency obviously was shortened ($P < 0.05$), and the number of errors obviously was increased ($P < 0.05$) in aging mice. Interestingly, the changes in aging mice were alleviated after treatment with EA and N-BAI fractions of *Z. bungeanum*, as indicated by longer latency and fewer errors ($P < 0.05$).

Morris water maze test was also used to assess the learning and memory abilities of mice (Fig. 1C – 1F). In the orientation navigation test, all groups exhibited a shorter escape latency with the increase in training days ($P < 0.0001$, F [4, 174] = 10.89). However, the escape latency of aging mice was significantly longer than the control mice ($P < 0.01$, F [1, 50] = 10.40), indicating that the learning and memory abilities were significantly impaired in aging mice. But EA ($P = 0.0144$, F [1, 50] = 4.242) and N-BAI ($P = 0.0447$, F [4, 49] = 3.460) treatments shortened the escape latency of aging mice. In the spatial search test, aging mice displayed fewer the number of passing the platform zone and residence time in the target quadrant than the control group ($P < 0.01$), suggesting that the spatial memory of aging mice was damaged, and these changes can be ameliorated by hydergine treatment. Meanwhile, EA and N-BAI treatment reversed distinctly the D-gal-induced decrease in the number of passing the platform and residence time in the target quadrant ($P < 0.05$). Collectively, these results manifested that EA and N-BAI ameliorated amnesia in aging mice, which may act as an inhibitor of cognitive impairment in aging mice.

3.2 Effects of EA and N-BAI fractions on pathological damage and number of surviving neurons in hippocampus and cortex in aging mice.

To examine whether pathological was altered in the hippocampus of aging mice compared with normal mice and whether EA and N-BAI could defend it, HE staining was employed to analyze the morphology and number of survival hippocampal CA1 and CA3 neurons in different groups (Fig. 1G). The administration of D-gal induced a significant pathological injury of neurons in the hippocampus, characterized by atrophy, loose arrangement, and decreased number of neurons ($P < 0.01$). However, these changes were markedly halted by EA and N-BAI treatment ($P < 0.05$) (Fig. 1J and 1I). The immunohistochemistry for NeuN was used to label surviving neurons. The results revealed aging mice had a significantly reduced number of surviving neurons in the cortex ($P < 0.01$) (Fig. 1H and 1K).

Consistent with HE staining results, the number of positive neurons increased significantly in the EA and N-BAI treatment group compared with the aging mice. However, the number of surviving neurons in the EA group was higher than that in the N-BAI group in HE staining and the immunohistochemistry of NeuN ($P < 0.05$), indicating that EA was the optimal fraction. The above studies showed that EA was a major activity part of *Z. bungeanum* extracts against age-related neural lesions.

3.3 Effects of EA fraction on oxidative damage and neuroinflammation in aging mice.

To understand the specific mechanism of the protective effect of EA in aging mice, we measured antioxidant enzyme activity, lipid oxide content, the expression of Iba1 and CD11b. As illustrated in Figs. 2A and 2B, the activity of SOD in the brain tissue was remarkably suppressed and the level of MDA was increased after exposure to D-gal compared with the control group ($P < 0.01$). However, after EA treatment, the phenomenon had been changed, indicating that EA could improve the redox balance of brain tissue in mice. To detect changes in microglia in aging mice, we performed immunolabelling of microglial marker Iba1. As shown in Figs. 2C and 2E, D-gal significantly increased Iba1 levels in the hippocampus CA1 regions ($P < 0.01$), but which was attenuated by EA ($P < 0.05$). Meanwhile, the CD11b protein expression, a marker of microglial activation, was increased in D-gal-induced aging mice compared with the control group ($P < 0.01$). EA treatment also inhibited the expression of CD11b compared with aging mice ($P < 0.05$) (Fig. 2D). Microglia is the main immune cells in the central nervous system, our results suggested that EA can alleviate microglial inflammation of the brain tissue in aging mice.

3.4 Effects of EA fraction on the activation of NLRP3 inflammasome and the pyroptosis of GSDMD-mediated in aging mice.

NLRP3 inflammasome and GSDMD-mediated pyroptosis play an important role in microglial inflammation response. To verify the effects of EA on the activation of NLRP3-inflammasome and the pyroptosis of GSDMD-mediated in aging mice, the associating protein expression was tested by western blotting (Fig. 3). As expected, the expression of NLRP3, cleaved caspase-1, and cleaved Gasdermin D (GSDMD-N) of brain tissue were significantly increased in aging mice ($P < 0.01$), inversely, those could remarkably down-regulated by EA ($P < 0.05$). The release of activated IL-18 and IL-1β was increased in aging mice compared with the control group ($P < 0.01$). Interestingly, the levels of these factors in aging mice were significantly depressed after EA treatment ($P < 0.05$). Besides, the dUTP nick-end labeling (Tunel) assay was used to detect and verify the pyroptosis. The results showed a noticeable increase in death of the hippocampus and cortex of aging mice compared to the normal mice, and EA exhibited significant suppression of Tunel positive staining (Fig. 3F). Our results demonstrated that EA could suppress the activation of NLRP3 inflammasome and the pyroptosis of GSDMD-mediated in aging mice.

3.5 Effects of EA fraction on NLRP3 inflammasome and pyroptosis in LPS + ATP treated BV-2 cells.

To further understand the effects of EA fraction on NLRP3 inflammasome and pyroptosis, the experiment that LPS + ATP induced NLRP3 activation and GSDMD-mediated pyrolysis was performed in BV-2 cells.

As illustrated in Fig. 4A, a significant toxic effect was observed after LPS + ATP treatment, evidenced by reduced cell viability in the LPS + ATP treated group compared with the control group ($P < 0.01$). Nevertheless, pretreatment with various doses of EA (5, 10, 20 μg/ml) increased the cell viability of BV-2 cells, demonstrating EA protected BV-2 cells from LPS + ATP induced cell death ($P < 0.05$). Moreover, levels of NLRP3 inflammasome and pyroptosis-associated proteins were measured (Fig. 4B). In Western blot assessment, the expression of NLRP3, cleavage capase-1, and GSDMD-N, the release of activated IL-18 and IL-1β were increased after LPS + ATP treatment. Nevertheless, these alternations were partially reversed by EA. These findings reflected that EA can inhibit the activation of NLRP3 inflammasome and GSDMD-mediated pyroptosis in LPS + ATP treated BV-2 cells.

3.6 The chemical composition of EA active fraction of Z. bungeanum extracts

To examine the potential material basis for the EA fraction of *Z. bungeanum* extracts. HPLC-MS/MS was used to analyze the chemical composition of the optimal EA fraction. As shown in Table 1, compounds were identified and grouped as follows: Quercetin-3β-D-glucoside (16.403%) was recognized as the main constituents, and other components including Hirsutrin (8.360%), Epicatechin (7.966%), Chlorogenic acid (6.065%), Quercetin (7.562%), Quercetin 7-rhamnoside (4.923%), etc. It is dominated by flavonoids and acids natural compounds in EA fraction, of which flavonoids are more than 70% and acids are about 20% of all compounds.

Table 1
High performance liquid chromatography-tandem mass spectrometry (HPLC-MS/MS) analysis results for EA fraction of *Z. bungeanum* extracts.

Rt	Compound	Formula	Peakarea (%) for EA
3.313	Trigonelline	$C_7H_7NO_2$	1.52844
3.584	D-(-)-Quinic acid	$C_7H_{12}O_6$	0.61121
5.244	Arbutin	$C_{12}H_{16}O_7$	1.11925
7.676	Neochlorogenic acid	$C_{16}H_{18}O_9$	4.58405
7.787	Indole-3-acrylic acid	$C_{11}H_9NO_2$	1.29549
8.592	Chlorogenic acid	$C_{16}H_{18}O_9$	6.06548
8.754	Procyanidin B1	$C_{30}H_{26}O_{12}$	2.62687
8.965	1-Caffeoylquinic acid	$C_{16}H_{18}O_9$	2.18393
9.275	(+)-Magnoflorine	$C_{20}H_{23}NO_4$	2.65146
9.54	Epicatechin	$C_{15}H_{14}O_6$	7.96623
12.511	Rutin	$C_{27}H_{30}O_{16}$	4.00945
14.18	Quercetin	$C_{21}H_{20}O_{12}$	7.56245
14.212	Quercetin-3β-D-glucoside	$C_{21}H_{20}O_{12}$	16.40303
14.847	Hirsutrin	$C_{21}H_{20}O_{12}$	8.35987
15.182	Hyperoside	$C_{21}H_{20}O_{12}$	0.98516
16.208	Quercetin-3-Arabinoside	$C_{20}H_{18}O_{11}$	1.49379
16.387	Trifolin	$C_{21}H_{20}O_{11}$	1.53990
16.527	Avicularin	$C_{20}H_{18}O_{11}$	1.46737
16.662	Quercetin-3-D-xyloside	$C_{20}H_{18}O_{11}$	1.43884
16.737	Isorhamnetin-3-O-nehesperidine	$C_{28}H_{32}O_{16}$	0.61346
16.903	Quercetin-7-rhamnoside	$C_{21}H_{20}O_{11}$	4.92280
16.905	Morin	$C_{15}H_{10}O_7$	2.50276

Discussion

Z. bungeanum is plant-based food and traditional medicines, growing researches have demonstrated its potential in cognitive dysfunction [21]. In the present study, we demonstrated rich-bioflavonoids EA fraction is the optimal fraction of *Z. bungeanum* in inhibiting age-related cognitive decline. We furtherly found that EA fraction relieved oxidative damage, silenced the NLRP3 inflammasome, and restraining pyroptotic death in vivo and in vitro, which suggested the potential for *Z. bungeanum* in prevention and therapy for oxidative stress and neuroinflammation. Amusing, to the best of our knowledge, our work is the first systemic report of the presence of pyroptosis of the brain in D-gal-induced aging mice, although the neuroinflammation pathway has been reported [22]. In addition, GSDMD-mediated pyroptotic signaling pathway regulated by *Z. bungeanum* is also first reported here.

Aging is one of the most important risk factors for various neurodegenerative diseases. D-gal is a reducing sugar found in humans and foods [23]. Low doses of D-gal can excrete from the body, but at high levels, it can be converted into aldose and hydroperoxide under the catalysis of galactose oxidase, resulting in the generation of ROS, which may subsequently cause oxidative stress and inflammation [24]. Injection of D-gal into mice could induce changes that resembled accelerated brain aging, characterized by cognitive function impairment [22]. Nowadays, D-gal-induced brain aging is established to be beneficial for age-related neurodegenerative diseases study. In this experiment, the passive avoidance test and the Morris water maze test were used to evaluate the cognition of the D-gal-treated aging mice. Hydergine be widely used for treating patients with either dementia or 'age-related' cognitive symptoms [25], therefore, it was tested as the positive control in the present study. The work showed that the EA fraction of *Z. bungeanum* extracts could significantly improve cognitive dysfunction, relieve pathological injury in D-gal-induced aging mice. Consequently, EA is the optimal fraction of *Z. bungeanum* extracts to ameliorate cognitive deficits in aging mice. In addition, HPLC-MS/MS was used to analyze the composition of EA, the results showed that EA mainly contained chemical components of flavonoids. Flavonoids are common ingredients of numerous plants, which have a broad range of pharmacological activities, including anti-aging, antioxidant, anti-inflammatory, protect liver, etc [26, 27]. This also explained the EA fraction of *Z. bungeanum* can act as an age-related cognitive decline inhibitor.

In the following we explored the neuroprotective mechanisms by which EA fraction acts. Our results reflected that EA fraction could reverse the increase of lipid peroxides and the decrease of antioxidant enzyme activity induced by D-galactose. This is consistent with our previous researches [17]. The accumulation of excessive oxidative stress causes neuroinflammation in the brain, which subsequently impairs cellular activity and destabilizes neuronal homeostasis, ultimately leading to neuronal loss. Significantly, microglia are detectors of inflammation in the central nervous system. In healthy brains, microglia exist in a resting state. When exposed to pathological injury, microglia changed from a resting stage to activated phases. Some protein expression changes, such as CD11b and CD68, have been used as markers of microglia activation [28]. We monitored the effects of EA fraction on D-gal-induced morphological changes in Iba1-immunoreactive microglia and CD11b immunoblotting. Results showed EA can suppress oxidative damage and microglial activation in aging mice induced by D-gal.

Inflammatory signals can induce the production of inflammasomes. The NLRP3 inflammasome is the mainly studied inflammasome, which is a critical factor to initiate the process of neurodegeneration [29]. Mounting evidence suggests that administration of D-gal shows aging neuroinflammation phenotypes, such as microglial activation, increases of IL-1β, IL-6, and TNF-α levels, and activation of NLRP3 inflammasomes [30]. The results are entirely consistent with our research. Previous studies also have shown that *Z. bungeanum* extract inhibited the expression of TNF-α, IL-1β, and IL-12, and the activation of NLRP3 in dextran sulfate sodium-induced murine experimental colitis [31, 32]. Consistent with the results, our study demonstrated that the activation of NLRP3 inflammasome was inhibited by EA active fraction in the brain of D-gal-induced aging mice and BV-2 cells induced by LPS + ATP.

Cell death and inflammation are fundamental characteristics in the initiation and development of neurological dysfunction. GSDMD-mediated pyroptosis plays crucial roles in the pathogenesis of multiple neurological diseases and age-related degeneration [33–35]. Pyroptosis is a type of lytic programmed cell death, distinguished from apoptosis and necrosis [8, 36]. When the body is subjected to noxious stimuli, inflammasomes formation through caspase-1-dependent and/or caspase-4/5/11-dependent pyroptosis-signaling pathways activation may be triggered via intracellular and extracellular signaling pathways [37]. Next, gasdermin D (GSDMD), the pyroptosis executioner, as a substrate of both caspase-1 and caspase-11/4/5, releasing several inflammatory mediators such as IL-1β and IL-18 and leading to cell pyroptosis [8]. In this study, we found that neurons displayed characteristic features of pyroptosis in the brain of D-gal-induced aging mice, as evidenced by increased levels of caspase-1, IL-1β, IL-18, GSDMD-N, and Tunel-positive cells.

It is noteworthy that the specific role of pyroptosis has not yet been fully elucidated in D-gal-induced aging mice. The activation of NLRP3 inflammasome and GSDMD-mediated pyroptosis induced by LPS + ATP in BV-2 cells [38]. The pro-caspase-1 can indirectly connect with the adaptor protein apoptosis-associated speck-like protein (ASC), which combines with a pattern recognition receptor to form a macromolecular complex, known as inflammasomes [39]. After the activation of inflammasomes, pro-caspase-1 is cleaved to form active caspase-1, which may cleave the GSDMD protein molecule to form active N-terminal kinase portions to cause cell membrane perforation [40]. And baicalin has been reported to have a wide range of anti-inflammatory activities, blocking the NLRP3-GSDMD signaling in vitro [41]. Therefore, baicalin was tested as the positive control in LPS + ATP induced BV-2 cells. The result of the experiment in vitro was in correspondence with that of the experiment in vivo, activation of NLRP3 inflammasome and GSDMD-mediated pyroptosis signaling were inhibited by EA fraction in BV-2 cells induced by LPS + ATP. These works proved that EA fraction suppressed microglial pyorptosis by inhibiting the activation of NLRP3 inflammasomes.

Conclusions

Collectively, rich-bioflavonoids EA fraction was a potential candidate responsible for the elite therapeutic potential of age-related cognitive deficits, the mechanism of action is related to inhibiting oxidative stress, the activation of NLRP3 inflammasome, and GSDMD-mediated pyroptosis. A detailed illustration of the

study is shown in Fig. 5. However, our study still has a few limitations. Firstly, the active components in the EA fraction have not been further identified. Besides, our experiments focus on the classical pathway of pyroptosis, and the non-classical pathway remains to be explored. Next, our team will carry out in-depth research on these problems.

Abbreviations

PE: petroleum ether; DCM: methylene chloride; EA: ethyl acetate; N-BAI: n-butanol; LPS: Lipopolysaccharide; ATP: adenosine triphosphate; AD: Alzheimer's disease; PD: Parkinson's disease; D-gal: D-galactose; NLRP3: NLR3 family pyrin domain containing 3; ROS: Reactive oxygen species; IL-1β: Interleukin-1β; IL-18: Interleukin-18; GSDMD: gasdermin D; SEM: standard error of the mean; ANOVA: analysis of variance; Iba1: ionized calcium binding adapter molecule 1; CD11b: Mac-1, alphaM integrin, Cr3, MO-1, C3bi Receptor; SOD: Superoxide dismutase; MDA: malondialdehyde; Tunel: dUTP nick-end labeling.

Declarations

Funding

This research was supported by the Applied Basic Research Project of Sichuan Province (No. 21YYJC0301), the Key Research and Development Plan of Sichuan Province (No. 19ZDYF0600), and Xinglin Scholar Research Premotion Project of Chengdu University of TCM (No. CXTD2018013).

Availability of data and materials

The datasets and materials supporting the conclusions of this article are included within the article.

Competing interests

The authors declare that they have no conflict of interest.

Consent for publication

Not applicable.

Authors' Contributions

Meihuan Zhao performed the methodology, the practical work and drafted the manuscript; Yuan Dai validation and supervision; Ping Li completed western blotting analyses; Jie Wang completed HPLC-MS/MS analyses; Tengyun Ma did the data curation; Shijun Xu conceived, designed the study and critically reviewed, edited, and revised the paper contributed the conception and design of the study.

Ethics approval and consent to participate

All animal experiments were performed according to the National Institutes of Health Guide for the Care and Use of Laboratory Animals, and the Institute of Material Medica Integration and Transformation for Brain Disorders ethics committee approved the animal protocols.

Acknowledgements

The authors are grateful for the assistance of all staff of the Institute of Material Medica Integration and Transformation for Brain Disorder.

References

1. Gallagher, M., et al., What are the threats to successful brain and cognitive aging. Neurobiol Aging, 2019. 83: p. 130-134.
2. The 2015 Revision of the UN's World Population Projections. Population and Development Review, 2015. 41(3).
3. Mrak, R.E., S.T. Griffin, and D.I. Graham, Aging-associated changes in human brain. J Neuropathol Exp Neurol, 1997. 56(12): p. 1269-75.
4. Block, M.L. and J.S. Hong, Microglia and inflammation-mediated neurodegeneration: multiple triggers with a common mechanism. Prog Neurobiol, 2005. 76(2): p. 77-98.
5. Wu, Q., et al., MLKL Aggravates Ox-LDL-Induced Cell Pyroptosis via Activation of NLRP3 Inflammasome in Human Umbilical Vein Endothelial Cells. Inflammation, 2020. 43(6): p. 2222-2231.
6. Zhang, X., et al., Oligodendroglial glycolytic stress triggers inflammasome activation and neuropathology in Alzheimer's disease. Sci Adv, 2020. 6(49).
7. Guo, H., J.B. Callaway, and J.P. Ting, Inflammasomes: mechanism of action, role in disease, and therapeutics. Nat Med, 2015. 21(7): p. 677-87.
8. Shi, J., W. Gao, and F. Shao, Pyroptosis: Gasdermin-Mediated Programmed Necrotic Cell Death. Trends Biochem Sci, 2017. 42(4): p. 245-254.
9. Zhao, N., et al., Amentoflavone suppresses amyloid β1-42 neurotoxicity in Alzheimer's disease through the inhibition of pyroptosis. Life Sci, 2019. 239: p. 117043.
10. Li, H., et al., Quercetin improves cognitive disorder in aging mice by inhibiting NLRP3 inflammasome activation. Food Funct, 2020.
11. de Araújo, F.M., et al., Role of Microgliosis and NLRP3 Inflammasome in Parkinson's Disease Pathogenesis and Therapy. Cell Mol Neurobiol, 2021.
12. Kraft, A.D. and G.J. Harry, Features of microglia and neuroinflammation relevant to environmental exposure and neurotoxicity. Int J Environ Res Public Health, 2011. 8(7): p. 2980-3018.
13. Ju, S., et al., Oral administration of hydrolyzed red ginseng extract improves learning and memory capability of scopolamine-treated C57BL/6J mice via upregulation of Nrf2-mediated antioxidant mechanism. J Ginseng Res, 2021. 45(1): p. 108-118.

14. Livingston, G., et al., Dementia prevention, intervention, and care: 2020 report of the Lancet Commission. Lancet, 2020. 396(10248): p. 413-446.
15. Zhang, M., et al., Hydroxy-α-sanshool isolated from Zanthoxylum bungeanum attenuates learning and memory impairments in scopolamine-treated mice. Food Funct, 2019. 10(11): p. 7315-7324.
16. Li, R.L., et al., Hydroxy-α-sanshool Possesses Protective Potentials on H(2)O(2)-Stimulated PC12 Cells by Suppression of Oxidative Stress-Induced Apoptosis through Regulation of PI3K/Akt Signal Pathway. Oxid Med Cell Longev, 2020. 2020: p. 3481758.
17. Zhao, M., et al., Bungeanum Improves Cognitive Dysfunction and Neurological Deficits in D-Galactose-Induced Aging Mice via Activating PI3K/Akt/Nrf2 Signaling Pathway. Front Pharmacol, 2020. 11: p. 71.
18. Wei, J.P., et al., Drinking water temperature affects cognitive function and progression of Alzheimer's disease in a mouse model. Acta Pharmacol Sin, 2021. 42(1): p. 45-54.
19. Luo, M.L., et al., Transplantation of NSCs Promotes the Recovery of Cognitive Functions by Regulating Neurotransmitters in Rats with Traumatic Brain Injury. Neurochem Res, 2019. 44(12): p. 2765-2775.
20. Fan, Z., et al., Tenuigenin protects dopaminergic neurons from inflammation via suppressing NLRP3 inflammasome activation in microglia. J Neuroinflammation, 2017. 14(1): p. 256.
21. Zhang, M., et al., Zanthoxylum bungeanum Maxim. (Rutaceae): A Systematic Review of Its Traditional Uses, Botany, Phytochemistry, Pharmacology, Pharmacokinetics, and Toxicology. Int J Mol Sci, 2017. 18(10).
22. Oskouei, Z., et al., Evaluation of the effect of thymoquinone in d-galactose-induced memory impairments in rats: Role of MAPK, oxidative stress, and neuroinflammation pathways and telomere length. Phytother Res, 2020.
23. Acosta, P.B. and K.C. Gross, Hidden sources of galactose in the environment. Eur J Pediatr, 1995. 154(7 Suppl 2): p. S87-92.
24. Ullah, F., et al., Caffeine prevents d-galactose-induced cognitive deficits, oxidative stress, neuroinflammation and neurodegeneration in the adult rat brain. Neurochem Int, 2015. 90: p. 114-24.
25. Olin, J., et al., Hydergine for dementia. Cochrane Database Syst Rev, 2000(2): p. Cd000359.
26. Yi, Y.S., Flavonoids: Nutraceuticals for Rheumatic Diseases via Targeting of Inflammasome Activation. Int J Mol Sci, 2021. 22(2).
27. Ma, Y., et al., Flavonoid-Rich Ethanol Extract from the Leaves of Diospyros kaki Attenuates D-Galactose-Induced Oxidative Stress and Neuroinflammation-Mediated Brain Aging in Mice. Oxid Med Cell Longev, 2018. 2018: p. 8938207.
28. Mee-Inta, O., Z.W. Zhao, and Y.M. Kuo, Physical Exercise Inhibits Inflammation and Microglial Activation. Cells, 2019. 8(7).
29. Zhao, Z., et al., A novel role of NLRP3-generated IL-1β in the acute-chronic transition of peripheral lipopolysaccharide-elicited neuroinflammation: implications for sepsis-associated

neurodegeneration. J Neuroinflammation, 2020. 17(1): p. 64.
30. Shwe, T., et al., D-galactose-induced aging does not cause further deterioration in brain pathologies and cognitive decline in the obese condition. Exp Gerontol, 2020. 138: p. 111001.
31. Zhang, Z., et al., Zanthoxylum bungeanum pericarp extract prevents dextran sulfate sodium-induced experimental colitis in mice via the regulation of TLR4 and TLR4-related signaling pathways. Int Immunopharmacol, 2016. 41: p. 127-135.
32. Zhang, Z., et al., In Vivo Study of the Efficacy of the Essential Oil of Zanthoxylum bungeanum Pericarp in Dextran Sulfate Sodium-Induced Murine Experimental Colitis. J Agric Food Chem, 2017. 65(16): p. 3311-3319.
33. McKenzie, B.A., V.M. Dixit, and C. Power, Fiery Cell Death: Pyroptosis in the Central Nervous System. Trends Neurosci, 2020. 43(1): p. 55-73.
34. Govindarajan, V., J.P. de Rivero Vaccari, and R.W. Keane, Role of inflammasomes in multiple sclerosis and their potential as therapeutic targets. J Neuroinflammation, 2020. 17(1): p. 260.
35. Tong, Y. and S. Wang, Not All Stressors Are Equal: Mechanism of Stressors on RPE Cell Degeneration. Front Cell Dev Biol, 2020. 8: p. 591067.
36. Kovacs, S.B. and E.A. Miao, Gasdermins: Effectors of Pyroptosis. Trends Cell Biol, 2017. 27(9): p. 673-684.
37. Liu, X., et al., Inflammasome-activated gasdermin D causes pyroptosis by forming membrane pores. Nature, 2016. 535(7610): p. 153-8.
38. Li, Y., et al., Isoliquiritin ameliorates depression by suppressing NLRP3-mediated pyroptosis via miRNA-27a/SYK/NF-κB axis. J Neuroinflammation, 2021. 18(1): p. 1.
39. Schneider, K.S., et al., The Inflammasome Drives GSDMD-Independent Secondary Pyroptosis and IL-1 Release in the Absence of Caspase-1 Protease Activity. Cell Rep, 2017. 21(13): p. 3846-3859.
40. Aachoui, Y., et al., Inflammasome-mediated pyroptotic and apoptotic cell death, and defense against infection. Curr Opin Microbiol, 2013. 16(3): p. 319-26.
41. Shi, H., et al., Baicalin attenuates hepatic injury in non-alcoholic steatohepatitis cell model by suppressing inflammasome-dependent GSDMD-mediated cell pyroptosis. Int Immunopharmacol, 2020. 81: p. 106195.

Figures

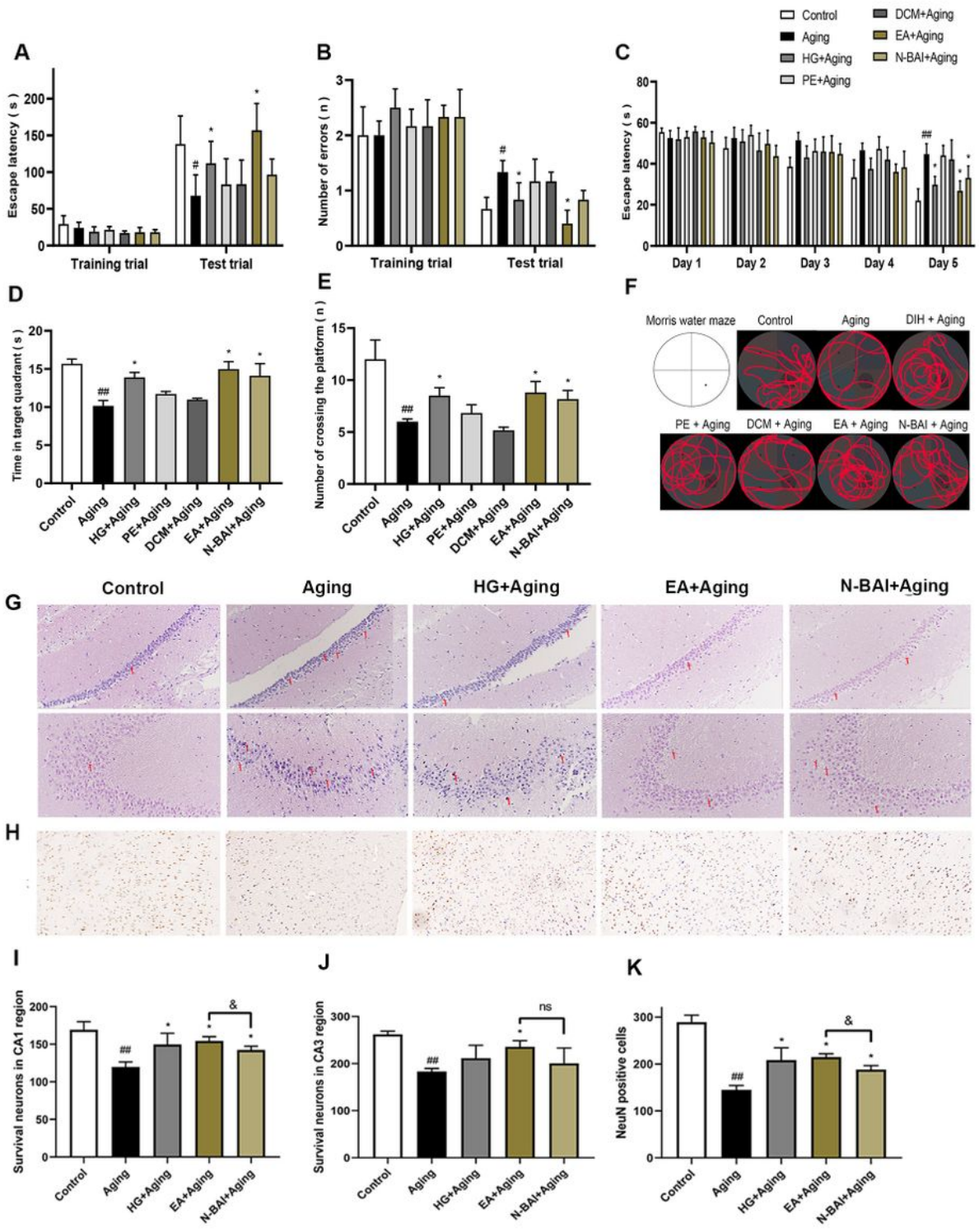

Figure 1

Screening the optimal part of four fraction of Z. bungeanum to improve cognitive function in D-galactose induced aging mice. The cognitive performance of mice in the passive avoidance test (A-B) and in the Morris water maze (C-F), as determined by the escape latency (A) and the number of errors (B) on the passive avoidance test of mice, the escape latency (C), representative traces of each group (D), swimming time in the target quadrant (E) and the number of passing the platform (F) in the Morris water

maze test. Representative pictures of hematoxylin–eosin (HE) staining in hippocampus CA1 and CA3 regions (G), quantifcation of neuronal survival in the hippocampal CA1 region (I) and CA3 region (J). Representative pictures of NeuN staining in cortex (H), and quantifcation of positive neurons in cortex (K). Scale bars = 50 μm. All data in A-F are presented as mean value ± SEM for n=6. Data in G-K are presented as mean value ± SEM for n = 4, ##P< 0.01 versus the control group, *P < 0.05 versus the model group, &P < 0.05 is the comparison between EA and N-BAI. Comparison of escape latency was performed by two-way analysis of variance (ANOVA) in the Morris water maze during the five consecutive days training trial days, Student's test was used for comparison between EA and N-BAI groups, others were performed by one-way analysis of variance (ANOVA).

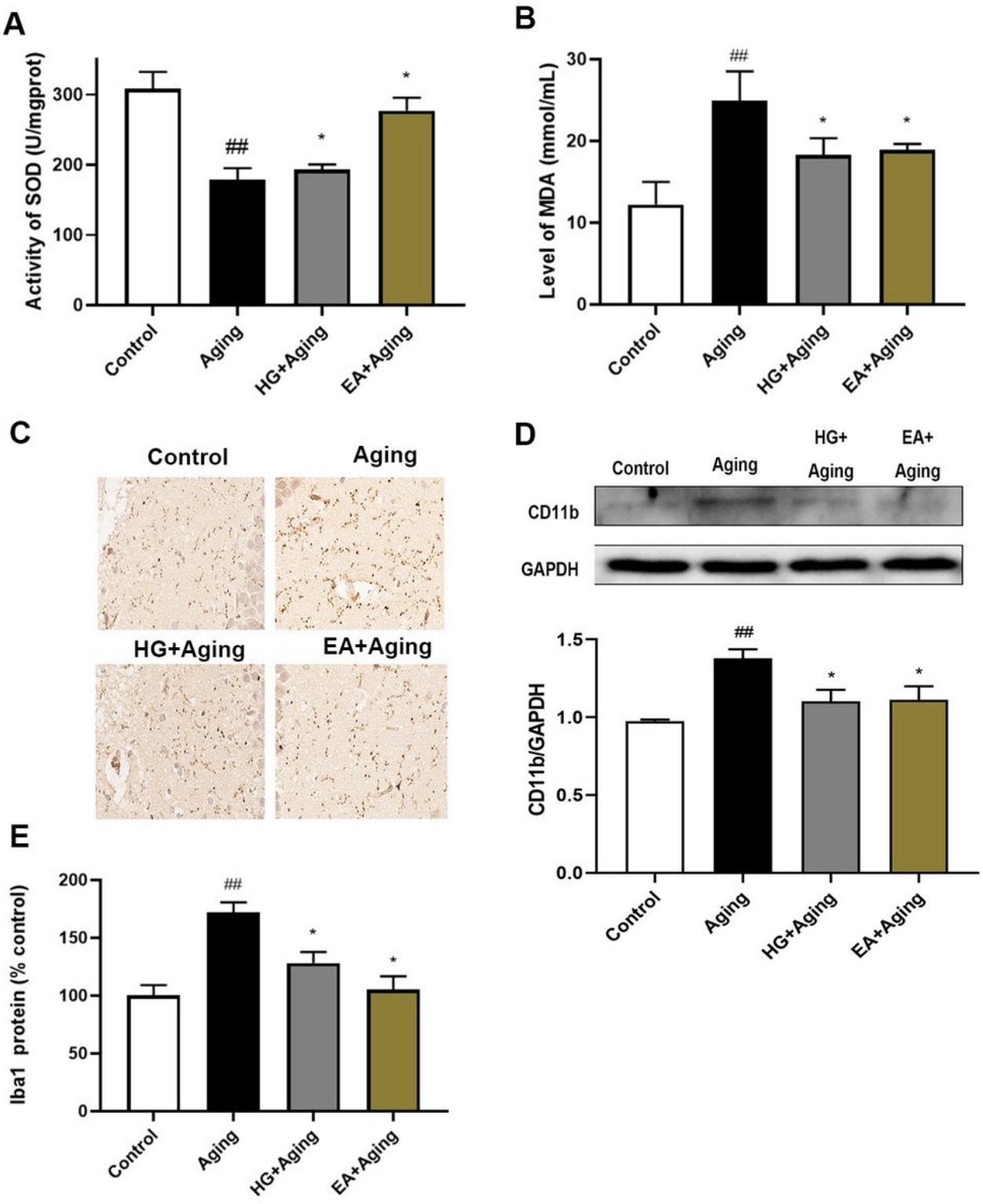

Figure 2

Effects of EA fraction on oxidative damage and neuroinflammation in D-galactose induced aging mice. Effects of EA on superoxide dismutase (SOD) activities (A), malondialdehyde (MDA) levels (B). Representative immunohistochemical images of Iba1 in the hippocampal CA1 regions of mice (C), quantifcation of Iba1 positive neurons (E). Western blot and quantitative analysis the protein expression of CD11b, GAPDH was used as loading control (D). Scale bars = 25 μm. All dates are presented as mean

value ± SEM for n = 5, ##P< 0.01 versus the control group, *P < 0.05 versus the model group. All dates were performed by one-way analysis of variance (ANOVA).

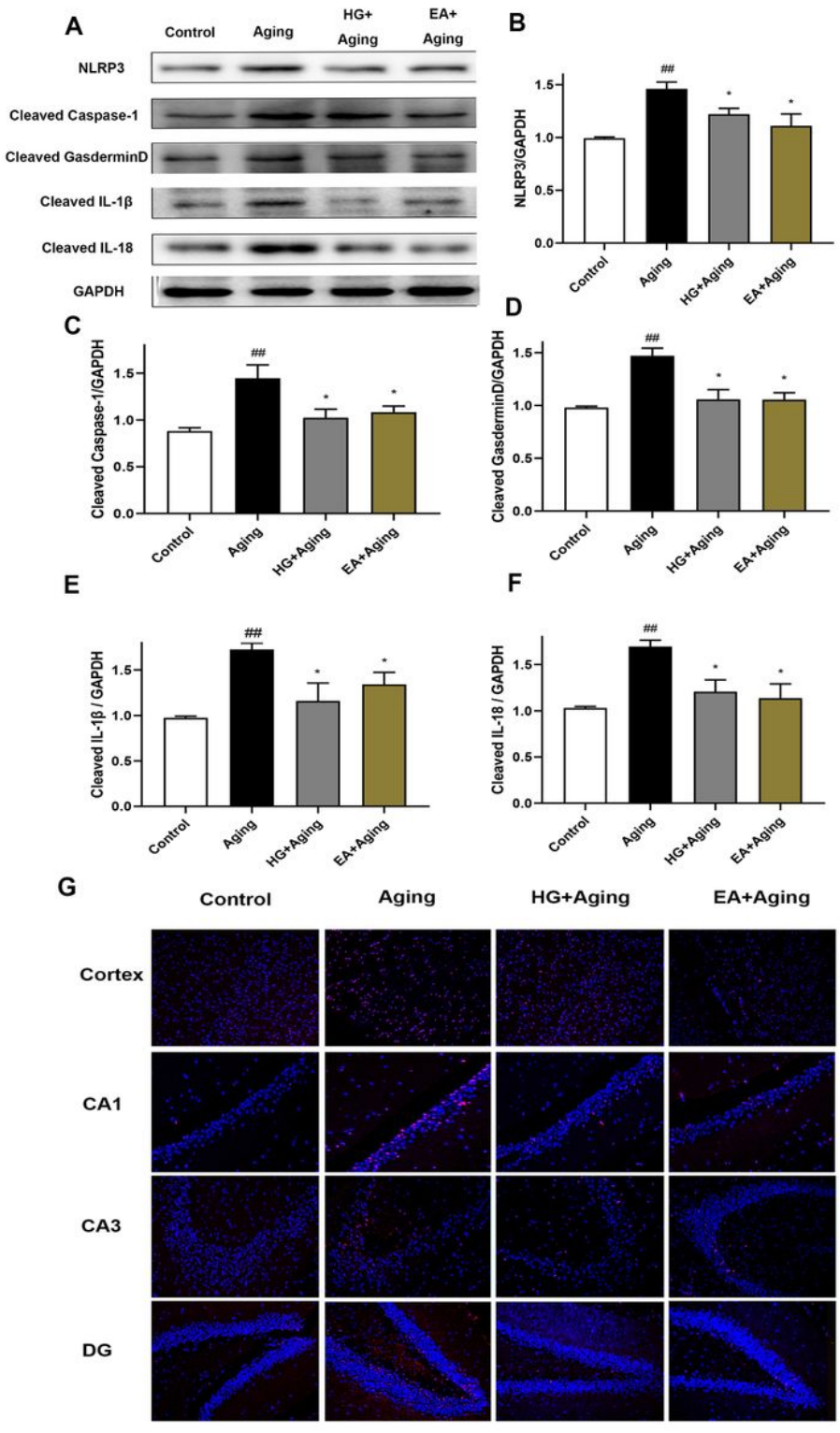

Figure 3

Effects of EA fraction on NLRP3-dependent inflammasome activation and GSDMD-mediated pyroptotic in D-galactose induced aging mice. Western blotting was used to further examine the NLRP3, cleaved caspase-1, cleaved GasedrminD (GSDMD-N), cleaved IL-1β and cleaved IL-18 protein expression (A). And

Western blot and quantitative analysis of NLRP3, cleaved caspase-1, GSDMD-N, cleaved IL-1β, cleaved IL-18 protein in brain tissues, GAPDH was used as loading control (B-F). pyroptotic cell death was estimated by TUNEL staining (G). All dates are presented as mean value ± SEM for n = 3, ##P< 0.01 versus the control group, *P < 0.05 versus the model group. All dates were performed by one-way analysis of variance (ANOVA).

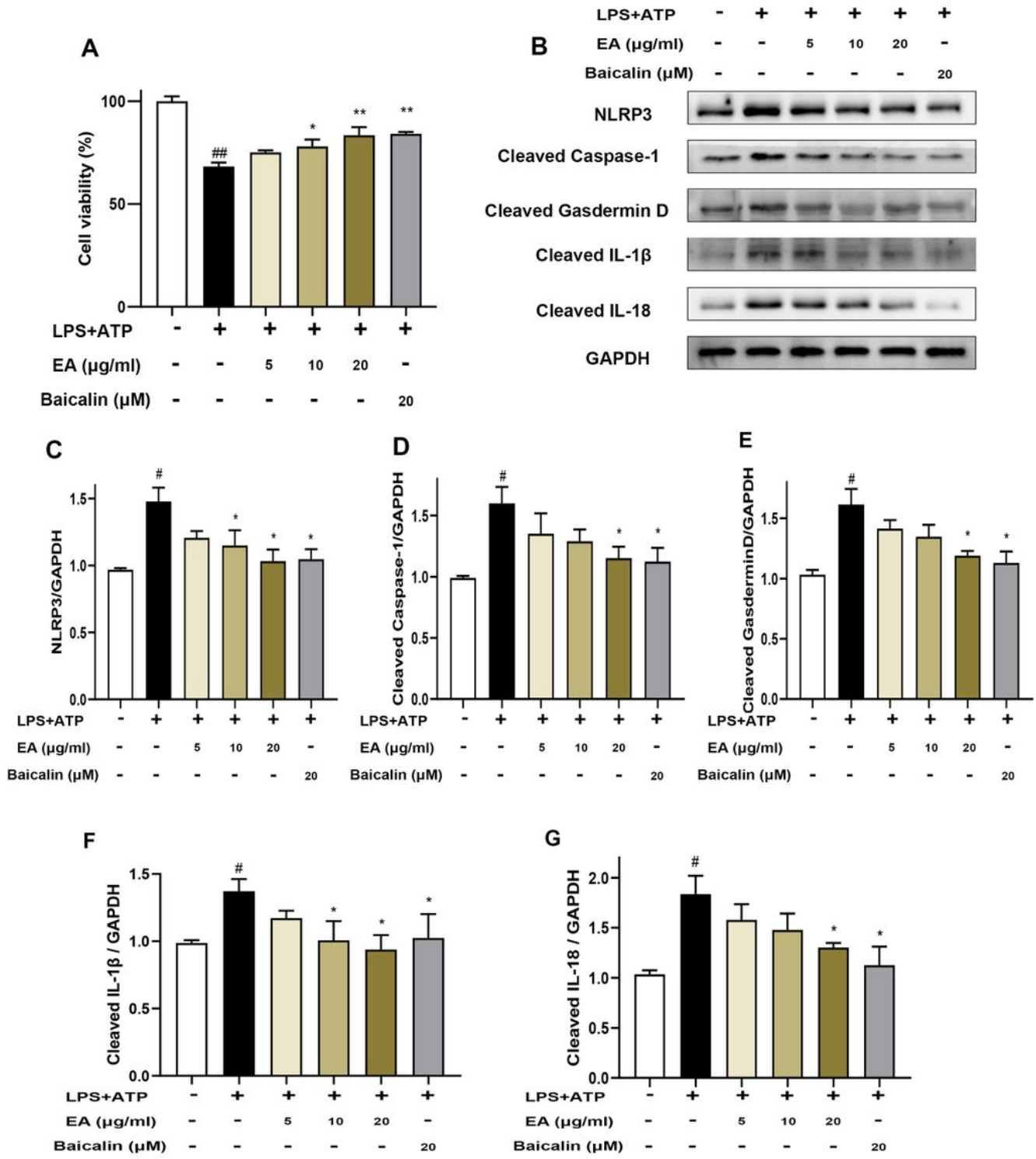

Figure 4

Effects of EA fraction on cell viability, NLRP3 inflammasome activation and GSDMD-mediated pyroptotic in LPS+ATP treated BV-2 cells. Cell viability (A), representative Western blots (B), and quantitative analysis of NLRP3, cleaved caspase-1, cleaved GasedrminD (GSDMD-N), cleaved IL-1β and cleaved IL-18 protein in LPS+ATP treated BV2 cells, GAPDH was used as loading control (C-G). All dates are presented as mean value ± SEM for n = 3, ##P< 0.01, #P< 0.05versus the control group, *P < 0.05 versus the LPS+ATP group. All dates were performed by one-way analysis of variance (ANOVA).

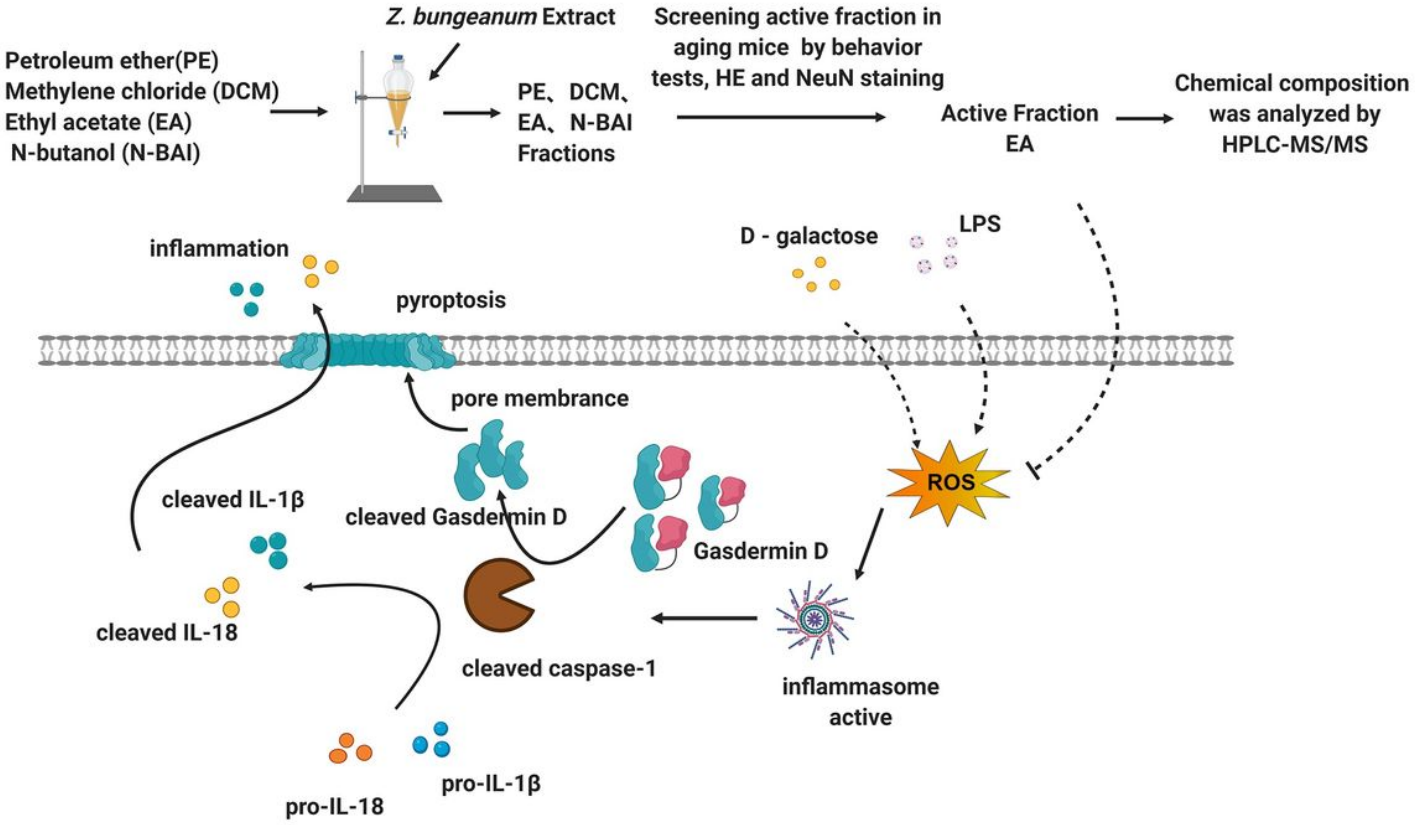

Figure 5

A schematic illustration of the research.